International Journal of Modern Manufacturing Technologies
ISSN 2067–3604, Vol. XIV, No. 2 / 2022
https://doi.org/ 10.54684/ijmmt.2022.14.2.294

# NUMERICAL SIMULATION OF ELASTIC-PLASTIC CONTACT WITH ISOTROPIC HARDENING

**Delia Cerlinca**[1,2], **Sergiu Spinu**[1,2]

[1] Department of Mechanics and Technologies, Stefan cel Mare University of Suceava,
13th University Street, 720229, Romania
[2] Integrated Center for Research, Development and Innovation in Advanced Materials, Nanotechnologies, and Distributed Systems for Fabrication and Control (MANSiD), Stefan cel Mare University, Suceava, Romania

Corresponding author: Sergiu Spinu, sergiu.spinu@fim.usv.ro

***Abstract:*** The contacts of mechanical components transmit loads that lead to subsurface stresses developing in the contacting bodies. In an efficient tribological design, these stresses are expected to remain under the yield strength of the softer contacting material. When this condition is not met, plastic flow occurs in the softer body. Under the assumption of isotropic hardening, the yield strength increases with the development of additional plastic strains. As plastic flow processes are dissipative and therefore path dependent, the elastic-plastic problem is unsolvable through analytical endeavours, but can be approached with a numerical algorithm capable of simulating the loading history. The Betti's reciprocal theorem provides the theoretical framework for the application of superposition principle to elastic-plastic stresses and displacement. An algorithm consisting in three nested loops is assembled from the solutions of simpler problems: (1) the purely elastic rough contact problem, (2) the inclusion problem and (3) the problem of the plastic strain increment. The numerical simulations suggest that the residual stresses decrease the intensity of the total stresses, thus delaying additional plastic flow. With increasing load, the heart-shaped plastic strain volume advances toward the surface, enveloping a plastic core near the initial point of contact. Compared to the purely elastic case, the elastic-plastic pressure shows a flatter distribution, while the contact radius is increased.
***Key words:*** elastic-plastic contact, power law isotropic hardening, plastic strains, fast Fourier transform.

## 1. INTRODUCTION

The tribological processes arising in contacts between machine elements that are brought together and transmit force through a limited contact region are of critical importance for understanding contact fatigue, wear and damage. Whereas contact analyses pioneered in 1882 with the study of the elastic contact between two glass lenses, and its solution was derived by analogy, the few existing explicit solutions still exhibit strong limiting assumptions. Contacts with complicated geometry and/or complex material behaviour lack analytical solution and therefore numerical analyses is employed to advance the understanding of the contact processes. An important breakthrough in the numerical study of the elastic-plastic contact was achieved with the three-dimensional algorithm developed by Jacq et al. [1], based on the boundary element method [2] and on the two-dimensional algorithm for the rough elastic-plastic contact advanced by Mayeur [3]. The code was further improved by replacing different algorithm modules with more rapid counterparts or by considering more complicated material properties or contact scenarios. The contact with linear or power law hardening behaviour was studied by Wang and Keer, [4]. Boucly et al. [5] developed a semi-analytical three-dimensional thermal–elastic–plastic model, applicable for rolling and/or sliding contact. Liu and Wang [6] advanced analytical solutions to the problem of uniform eigenstrains in a cuboidal region, thus enabling fast and accurate analyses of inclusion problems and contact problems. The rolling and sliding contact between two asperities was modelled by Boucly et al. [7], whereas Nélias et al. [8] integrated the elastic-plastic code into a model for the prediction of wear, based on material removal during cyclic loading. The elastic-plastic sliding contact was analysed by Nélias et al. [9], whereas Nélias et al. [10] modelled the rolling of an elastic ellipsoid upon an elastic-plastic flat. The problem of the elasto-plastic contact of nominally flat surfaces was solved with the fast Fourier transform method by Chen et al. [11]. Chen et al. [12] investigated the effects of sliding speed, heat partition, and thermal softening in a thermomechanical analysis of elastoplastic bodies. Other more recent studies [13-16] also involve the numerical simulation of the elastic-plastic contact.

In this paper, state-of-the-art numerical analysis techniques based on the fast Fourier transform are assembled in an algorithm structured on three nested loops. The algorithm computational efficiency is

derived from the calculation of convolutions in the Fourier transform domain. The interaction between the residual stresses and those induced by the contact tractions, which can be fully recovered by unloading, is studied in detail.

## 2. CONTACT MODEL

When load is transmitted through a concentrated point contact, important gradients of elastic stresses occur in a close proximity of the initial point of contact. Whereas the stress state in every point is described by a second order tensor, a norm of the latter tensor such as the von Mises equivalent stress $\sigma_{VM}$, can be calculated and compared with the yield strength of the contacting material to examine the initiation of plastic flow. A purely elastic analysis is a prerequisite in any elastic-plastic simulation. When load is applied steadily from zero to a final value, the contact mechanics literature [17] divides the evolution of the elastic-plastic contact process into three stages: (I) the purely elastic range, (II) the elastic-plastic stage, and (III) the perfectly (fully) plastic one (see fig. 1). The criterion for stage I is that the load remains small enough so that the developed stresses do not reach the yield strength. In this purely elastic process, there exist linearity between stress and strain, the final state is independent of intermediate states, and the stress and displacement fields depend only on the load level. In case of unloading, all deformation is completely recovered. With further loading, when the norm of the stress tensor exceeds the yield strength $\sigma_Y$, plastic flow is initiated in the regions of maximum stress intensity, leading to development of a plastic core inside the elastic material, as depicted in figure 1, stage II.

It should be noted that in a non-conforming contact, the maximum equivalent stress is reached at a specific depth on the contact axis, and the plastic deformation initiates around the latter point. In this stage, the elastic and the plastic strains are of the same order of magnitude, but proportionality is lost. Due to the dissipative nature of plasticity, the final state cannot be determined solely on the base of the load level, as in the purely elastic stage. The entire elastic-plastic loading history influence the outcome. In case of an elastic unloading, the plastic deformation is not recovered and remains as a permanent residual state.

Further load increase causes the plastic zone to reach the surface, surrounding an elastic core, as shown in figure 1, stage III. The elastic material escapes by plastic flow to the sides of the indenter, and the stress remains practically constant. Severe contact conditions with heavy loading or large rates of the loading usually lead to a contact process in which the stage II can be neglected, thus the material can be assumed to swing from purely elastic (stage I) directly to perfectly plastic (stage III). However, such simplification is too strong when the load is not large or when the rate of the loading is small, such as in most well-designed mechanical contacts. This paper focuses on the simulation of the stage II, but the description of the purely elastic stage I is a prerequisite for the contact process description. Basic concepts and equations for the solution of the contact problem are reviewed in this section.

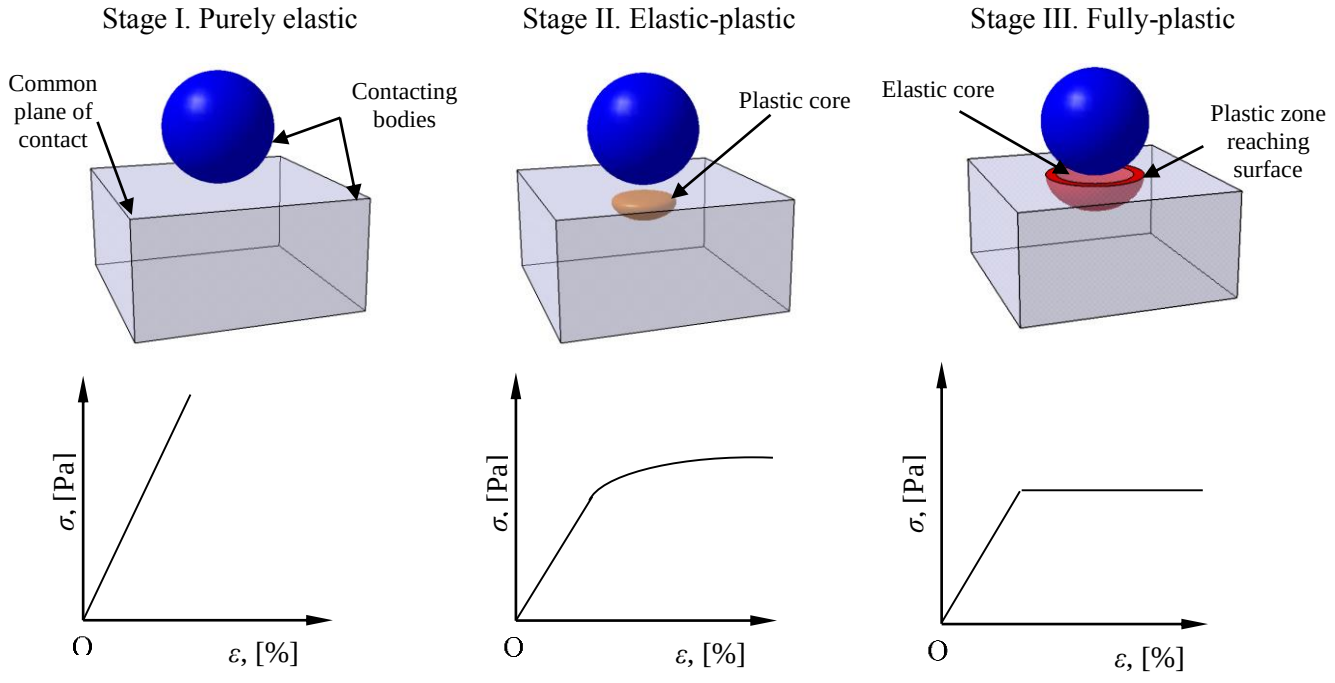


Fig.1. The stages in the plastic zone development and the schematic of the associated stress-strain ( $\sigma - \varepsilon$ ) relationship

The stare-of-the-art in the simulation of the elastic contact between bodies of arbitrary profiles was achieved with the computer algorithm developed by Polonsky and Keer [18], based on the general solution strategy developed in [17]. Three types of equations govern any contact model, regardless of the assumed behavior on the contacting materials (i.e., elastic, elastic-plastic, visco-elastic etc.): (a) the equation of deformation, (b) the static-force equilibrium and (c) the complementarity conditions, which are clearly identified in the system (1) written below. The involved parameters are: $u$ - the sum of normal displacements of points on the boundaries of both contacting bodies, assumed as elastic half-spaces, $hi$ - the contact geometry in undeformed state, $h$ - the gap (or clearance) between the deformed bodies, $\delta$ - the relative approach between the bulk bodies (also known as the rigid-body approach), and $W$ - the normal load. All these parameters are considered along the normal contact direction, perpendicular to the common plane of contact (see fig. 1).

A Cartesian coordinate system is attached, with the $xy$ plane matching the common plane of contact, and the origin in the initial point of contact. It should be noted that contact pressure $p$ and normal displacements are assumed parallel to the $z$-axis regardless of the bodies profiles, due to the fact that the contact region is small compared to dimensions of the contacting bodies, and therefore the bodies can be assumed [17] approximatively plane in the contact vicinity. These notations yield the following mathematical model:

$$\begin{aligned} &(a): \quad h = hi + u - \delta; \\ &(b): \quad \begin{cases} ha = 0; \\ p > 0 \quad on \quad \Gamma_C; \\ h > 0 \quad outside \quad \Gamma_C; \end{cases} \\ &(c): \quad W = \int_{-\infty}^{\infty}\int_{-\infty}^{\infty} p(x,y)dxdy, \end{aligned} \tag{1}$$

with $\Gamma_C$ the contact area. The algorithm input consists in: $W$, $hi$ and the parameters of the constitutive law for the contacting bodies (if purely elastic, the Young modulus $E$, the Poisson's ration $\nu$ or the shear modulus $\mu$). The sought output comprises $\Gamma_C$, $\delta$ and $p$. The latter can be further used to derive the stress state in the contacting bodies. An analytical solution for the system (1) cannot be achieved for arbitrary input, mainly because $\Gamma_C$ and $p$ are both unknown. The key to deriving the model solution by numerical approach is to obtain the displacement $u$ as a function of pressure and of the constitutive law for the materials of the contacting bodies. Further on, friction, shear stresses, various constitutive laws, or even material inhomogeneities can be treated by means of the system (1), provided the displacement is properly expressed.

Numerical analysis is required to obtain the needed displacement. Problem digitization replaces the continuous contact area with a reunion of rectangles on which pressure is assumed constant. A rectangular mesh is imposed in the common plane of contact, and representative points are chosen for each patch (usually the centers). System (1) is then written for each discrete point, resulting in a linear system of equations with the pressure matrix as unknown. The solution of the latter system can be achieved [18] with the aid of the Conjugate Gradient method, which provides the optimum computational efficiency.

It should be noted that the shape and location of the contact area is subject to iteration, as well as the solution of the linear system in pressure. The numerical calculation of displacement must be done at each iteration based on the current approximation of pressure. As the latter can be arbitrary, a method for calculation of displacement due to arbitrary pressure is needed, which is described in the following section.

## 3. ELASTIC DEPENDENCIES

By approximating the contacting bodies with elastic half-spaces, solutions derived in the half-space theory can be used, such as the Boussinesq result for a point force acting normally on the half-space boundary. Such solutions are referred to as the Green's functions, and are the counterpart of the unit impulse response in digital signal processing. The displacement is further expressed, in accordance with the superposition principle applicable in the frame of linear elasticity, as the superposition of effects of multiple point forces, resulting in an integral which is mathematically a convolution product between the Green's function $G$ and the pressure input:

$$u^p(x,y) = \int_{-\infty}^{\infty}\int_{-\infty}^{\infty} G(x-x', y-y')\, p(x',y')dx'dy' \,, \tag{2}$$

with $G(x,y) = 1/(\pi E^* \sqrt{x^2+y^2})$, and $E^*$ the contact compliance [17]. The digitization of equation (2) implies that: (1) the integral with infinite limits is substituted by summation on a finite domain chosen around the initial point of contact, (2) the pressure distribution is represented by a matrix of elements denoting the pressure values in all representative mesh nodes, and (3) a matrix of so-called influence coefficients substitutes the Green's function. If $2\Delta_i$, $i = x, y$, are the step sizes of the mesh, by defining the new variables $x_u = x + \Delta_x$, $x_\ell = x - \Delta_x$, $y_u = y + \Delta_y$,

$y_\ell = y - \Delta_y$, the function required to calculate the influence coefficients is:

$$D(x,y) = g(x_u, y_u) + g(x_\ell, y_\ell) - g(x_u, y_\ell) - g(x_\ell, y_u), \quad (3)$$

with $g(x,y) = \iint G(x,y)dxdy$. In relation (3), the function arguments should be replaced with all possible distances between the mesh nodes. E.g., consider a discrete observation point $(x_k, y_\ell)$ in which the displacement is calculated, and a discrete source point $(x_i, y_j)$ in which pressure is applied. The two are related through the influence coefficient $D(x_i - x_k, y_j - y_\ell)$, which expresses numerically the displacement induced in the observation point by a $1/(4\Delta_x\Delta_y)$ uniform pressure acting on the rectangular patch centered on the source point. The discrete counterpart of relation (2) can thus be expressed as a multi-summation over the $N_x \times N_y$ points in the mesh, i.e., a discrete convolution product:

$$u^p(x_i, y_j) = \sum_{k=1}^{N_x}\sum_{\ell=1}^{N_y} D(x_i - x_k, y_j - y_\ell)\, p(x_k, y_\ell), \quad (4)$$

with $i = 1 \ldots N_x$ and $j = 1 \ldots N_y$. It should be noted that in this multi-summation, every point in the mesh is considered as both source and observation point. Equation (4) provides means to calculate the displacement due to arbitrary pressure, as requested by the solution of the contact model (1). Efficient calculation of (4) is available with the Discrete Convolution Fast Fourier Transform Technique (DCFFT) [19,20].

In the same manner, the stresses in the contacting body due to pressure can be expressed as discrete convolutions of type (4). To this end, the surface mesh is extended inside the body, resulting in a set of cuboids in which all problem parameters are assumed constant and equal to the discrete value from the center. The six components of the stress tensor in every representative node $(x_i, y_j, z_k)$, $i = 1 \ldots N_x$, $j = 1 \ldots N_y$, $k = 1 \ldots N_z$, result as:

$$\sigma^p_{\varsigma\xi}(x_i, y_j, z_k) = \sum_{\ell=1}^{N_x}\sum_{m=1}^{N_y} S^p_{\varsigma\xi}(x_i - x_\ell, y_j - y_m, z_k)\, p(x_\ell, y_m), \quad (5)$$

with $\varsigma, \xi = x, y, z$. The influence coefficients needed in (5) are derived in the same manner as (3), by considering the appropriate Green's function, expressed in closed form in [17]. They also depend on depth, so that the calculation of stresses should be conveniently performed in layers of constant depth. Mathematically, $S^p_{\varsigma\xi}(x_i - x_\ell, y_j - y_m, z_k)$ expresses the $\varsigma\xi$ component of the stress tensor induced at the coordinates $(x_i, y_j, z_k)$ by a $1/(4\Delta_x\Delta_y)$ uniform pressure acting on the rectangular patch centered in $(x_\ell, y_m)$.

Relations (4) and (5) provide means to calculate stresses and displacements due to arbitrary pressure in an elastic contact. Additional relations will be derived in the following section to express the contribution of the plastic zone to the displacement and stress field in the elastic-plastic material.

## 4. ELASTIC-PLASTIC DEPENDENCIES

Superposition of effects can also be applied for the elastic-plastic material in the frame of the Betti's reciprocal theorem [1-3]. Two independent loads applied to an elastic body of boundary $\Gamma$ and volume $\Omega$ result in two states: the first one $(u, \varepsilon, \sigma)$ with an initial plastic strain $\varepsilon^p$ in a domain $\Omega_p$, and the second one $(u^*, \varepsilon^*, \sigma^*)$ with a unit point force applied along $z$ direction in a point $A$. Assuming $M$ is an integration point in surface or volume, it is found [1] that the total displacement $u$ can be expressed as:

$$u(A) = u^p(A) + u^r(A), \quad (6)$$

$$u^p(A) = \int_{\Gamma_C} u^*(M, p^*(A))\, p(M)d\Gamma, \quad (7)$$

$$u^r(A) = 2\mu \int_{\Omega_p} \varepsilon^p_{ij}(M)\varepsilon^*_{ij}(M, p^*(A))d\Omega, \quad (8)$$

where $u^*(M, p^*(A))$ is the normal displacement, and $\varepsilon^*_{ij}(M, p^*(A))$ the $ij$ component of the strain tensor, both induced in $M$ by the unit point force applied in $A$. If the latter is removed, $u^p$ is completely recovered, whereas $u^r$ persists. Thus, the total displacement in the body with plastic strains and surface pressure can be divided into a part due to pressure, and a part due to the plastic strains, also referred to as the residual part. Comparison of equations (7) and (2) leads to the idea that $u^*(M, p^*(A))$ is in fact the Green's function for the dependency of normal displacement on pressure, and therefore relation (4) can be applied in the calculation of (7). In the same manner, $\varepsilon^*_{ij}(M, p^*(A))$ can be regarded as a Green's function whose integration leads to the required influence coefficients $B_{\varsigma\xi}$ [1]. Equation (8) can also be written as a convolution product and calculated with DCFFT:

$$u^r(x_i, y_j, 0) = \sum_{\ell=1}^{N_x}\sum_{m=1}^{N_y}\sum_{n=1}^{N_z} B_{\varsigma\xi}\left(x_i - x_\ell, y_j - y_m, z_n\right)\varepsilon^p_{\varsigma\xi}(\ell, m, z_n), \quad (9)$$

A similar partition can be derived for stresses. If $M_{ijk\ell}$ denotes the fourth order tensor for elastic moduli, $M_{ijk\ell} = \lambda\delta_{ij}\delta_{k\ell} + \mu(\delta_{ik}\delta_{j\ell} + \delta_{i\ell}\delta_{jk})$, with $\lambda$ and $\mu$ the Lame's constants and $\delta_{ij}$ the Kronecker delta,

$$\sigma_{ij} = \sigma_{ij}^{p} + \sigma_{ij}^{r}, \tag{10}$$

$$\sigma_{ij}^{p} = M_{ijk\ell}\left(\frac{1}{2}(u_{k,\ell}^{p} + u_{\ell,k}^{p})\right), \tag{11}$$

$$\sigma_{ij}^{r} = M_{ijk\ell}\left(\frac{1}{2}(u_{k,\ell}^{r} + u_{\ell,k}^{r}) - \varepsilon_{k\ell}^{p}\right). \tag{12}$$

The symbol for the partial derivative $u_{k,\ell} = \partial u_k / \partial x_\ell$ is used in relations (11) and (12), with $k,\ell = 1,2,3$, and $\vec{x}_1 = \vec{x}$, $\vec{x}_2 = \vec{y}$ and $\vec{x}_3 = \vec{z}$. The stresses due to pressure in equation (11) are computed numerically in the same manner as (5), whereas the problem of residual stresses in equation (12), known as the inclusion problem, can also be treated with DCFFT. A detailed solution for the latter, together with explicit expressions for the required influence coefficients, can be found in [21]. The latter solution implies superposition of three elastic states: (1) a cuboid of uniform plastic strains in the infinite space, (2) its mirror image with respect to the half-space boundary, also considered in the infinite space, and (3) the free surface relief. For the state (1), a three-dimensional DCFFT algorithm can be applied. Solution of state (2) can also be achieved with a 3D DCFFT-type technique, but in which convolution is substituted by correlation in the depth direction. Finally, computational of state (3) is performed in the same manner as (5).

Thus, the superposition principle can be applied for the elastic-plastic body to derive the displacement and stresses due to both a recoverable elastic state, i.e., the surface pressure, and a persistent one, i.e., the plastic strains. The found dependencies and the type of DCFFT algorithms required to solve the elastic-plastic contact problem are reviewed in table 1.

Table 1. Elastic-plastic dependencies

| Dependency | Source domain | Observation domain | Computational strategy |
|---|---|---|---|
| $u^p = u^p(p)$ | 2D | 2D | 2D DCFFT |
| $u^r = u^r(\varepsilon^p)$ | 3D | 2D | 2D DCFFT in layers of constant depth |
| $\sigma^p = \sigma^p(p)$ | 2D | 3D | 2D DCFFT in layers of constant depth |
| $\sigma^r = \sigma^r(\varepsilon^p)$ | 3D | 3D | 3D DCFFT and 2D DCFFT |

In order to simulate the behavior of the elastic-plastic material with isotropic hardening, the von Mises yield criterion was used together with the Prandtl-Reuss equation [1] for the calculation of the plastic strain rate and the Swifts's law for the hardening curve. The yield function $f$ can be expressed in terms of the yield criterion and the accumulated plastic strain $e^p$, which is a measure of the historical plastic flow:

$$f(e^p) = \sigma_{VM} - \sigma_Y(e^p). \tag{13}$$

The case $f < 0$ corresponds to a purely elastic state, in which the increment of plastic strains is nil, $d\varepsilon^p = 0$. If $f = 0$, two situations are possible: (1) $df = 0$, corresponding to plastic flow, and (2) $df < 0$ indicating elastic unloading. In theory, $f > 0$ is not possible because the elastic domain of the material expands to accommodate the new stress state. This expansion, if independent of the sign of a new stress, is referred to as isotropic hardening. As opposed to kinematic hardening, in which the elastic expansion is observed only if the new stress holds the same sign as the original one. The isotropic hardening curve employed in this paper (the Swifts's law), uses three parameters *B, C, n* that can be derived experimentally:

$$\sigma_Y(e^p) = B(C + e^p)^n. \tag{14}$$

The finite increment of the accumulated plastic strain $\delta e^p$ corresponding to a new load increment is derived from the condition $f(e^p + \delta e^p) = 0$, which is solved as a non-linear equation in $\delta e^p$ by the Newton-Raphson numerical method. The increment of plastic strains $\delta\varepsilon_{ij}^p$ can then be calculated as [1]:

$$\delta\varepsilon_{ij}^p = \frac{3}{2}\delta e^p \frac{\sigma'_{ij}}{\sigma_{VM}}, \tag{15}$$

with $\sigma'_{ij}$ the deviatoric stress tensor components. The described dependencies will be assembled in the following section in an algorithm capable of solving the elastic-plastic contact problem.

## 5. ALGORITHM OVERVIEW

The algorithm for solving the contact model is built on three nested loops. The innermost loop is charged with the derivation of the plastic strain increment by Newton-Raphson iteration, the intermediate one with the calculation of the pressure distribution by

Conjugate Gradient method, and the outer one with the simulation of the loading history by applying the load in small steps. The dependency $\sigma^r = \sigma^r(\varepsilon^p)$, which is the most computationally intensive as both the source and the observation domains are three-dimensional, is inconveniently placed in the intermediate loop. The treatment of the involved multi-summations with DCFFT is critical in achieving a reasonable computational effort. The incremental load application is required only for $f \geq 0$, and stress formulas from the Hertzian framework can be used to estimate the maximum load for which the maximum equivalent stress is less but close to the yield strength. A detailed description of the algorithm, including specialized routines for solving the contact model (1) or the inclusion problem, is beyond the point of this paper, and only the main steps will be conceptually described:

1. Acquire the input data: elastic parameters E, $\nu$, parameters *B, C, n* for relation (14), contact geometry, maximum load level.
2. Establish a 3D computational domain around the initial point of contact, which is expected to encompass the contact area in the common plane of contact, and in depth the region with plastic strains. Choose the mesh parameters based on the available computational resources.
3. Apply the $k^{\text{th}}$ load increment. An upper index will be used in the following to denote the load increment for which the variable is calculated.
4.Solve the contact model (1) with a vanishing increment of plastic strains ($\delta\varepsilon_{ij}^{p(k)} = 0$), assisted by the Conjugate Gradient method (the intermediate loop):
4.1. Start the iteration with a uniform pressure as an initial approximation $p^{(k)}$ (this means that initially the whole computational domain is assumed in contact).
4.2. Compute the displacement due to pressure $u^{p(k)} = u^{p(k)}(p^{(k)})$.
4.3. Obtain the total displacement by superimposing the residual displacement corresponding to the previous load level: $u^{(k)} = u^{p(k)}(p^{(k)}) + u^{r(k-1)}(\varepsilon^{p(k-1)})$.
4.4. Solve the linear system in pressure resulting from digitization of equation (1)(a).
4.5. Iterate the contact area by removing patches with negative pressure and by adding patches with negative clearance (this results in a modification of the number of equations in the linear system from the previous step).
4.6. Force pressure elements to satisfy the static equilibrium (1)(c).
4.7. Verify convergence of pressure.
5. If convergence is reached, use the derived pressure to calculate subsurface stresses due to pressure $\sigma^{p(k)} = \sigma^{p(k)}(p^{(k)})$.
6.Obtain the total stresses by superimposing the residual stresses reached at the previous load increment: $\sigma^{(k)} = \sigma^{p(k)}(p^{(k)}) + \sigma^{r(k-1)}(\varepsilon^{p(k-1)})$.
7.Obtain the finite increment of the accumulated plastic strain $\delta e^{p(k)}$ (corresponding to the $k^{\text{th}}$ load increment) by Newton-Raphson iteration (i.e., the innermost loop).
8.Compute the increment of plastic strain $\delta\varepsilon_{ij}^{p(k)}$ according to (15).
9.Go to step 4 and re-solve the contact model by considering $\varepsilon^{p(k)}$ instead of $\varepsilon^{p(k-1)}$ (in other words, the increment of plastic strains $\delta\varepsilon_{ij}^{p(k)}$ is no longer assumed nil). The new relations for the residual part are: $u^{(k)} = u^{p(k)}(p^{(k)}) + u^{r(k)}(\varepsilon^{p(k)})$ and $\sigma^{(k)} = \sigma^{p(k)}(p^{(k)}) + \sigma^{r(k)}(\varepsilon^{p(k)})$.
10.Stop the code execution when pressure is stabilized with respect to the residual displacement, e.g. when the increment of residual displacement corresponding to the current load increment $u^{r(k)}(\delta\varepsilon^{p(k)})$ varies from one iteration to the next within an imposed precision.
11.Apply a new load increment and go to step 3 until the maximum loading level is attained.

## 6. SIMULATION EXAMPLE

The contact between a rigid ball of radius 18 mm and an elastic-plastic half-space is loaded up to a maximum level of 20 kN, resulting in an equivalent Hertzian pressure $p_H = 20\,\text{MPa}$ and a Hertzian contact radius $p_H = 1.054\,\text{mm}$, which are used as normalizers for stresses and coordinates, respectively. The computational domain is a cuboid of side lengths $1.5a_H \times 1.5a_H \times 1.6a_H$, divided into $128\times128\times120$ identical elementary cuboids. The elastic parameters for the half-space are fixed at $E = 210$ GPa, $\nu = 0.3$, whereas the hardening parameters in equation (14) are: $B = 1240\,\text{MPa}$, $C = 30$, $n = 0.085$. The process history is replicated with 20 equal load increments, starting from a load level of 1 kN. Figures 2-6 present the predicted distributions of stresses, pressure and plastic strains in the plane $y = 0$, attained at the end of the loading program. It was verified that increasing the number of load increments does not significantly affect the solution. The partition of stresses according to equation (10) is suggested by the iso-contours depicted in figures 2-4. The flattening of pressure and the peripheral advance of the plastic strain region

towards the free surface agree with the general theory [17] for the concentrated elastic-plastic contact.

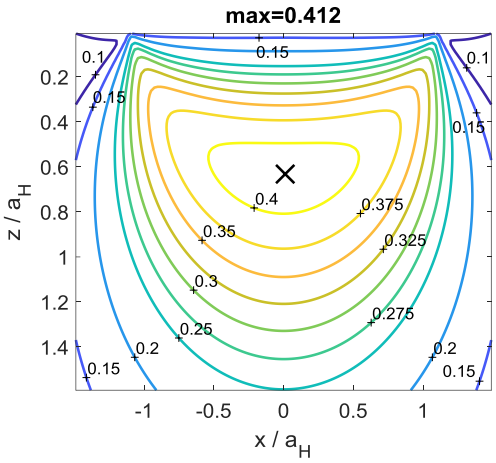


Fig. 2. Iso-contours of dimensionless equivalent von Mises stress due to pressure, $\sigma_{VM}^{p} / p_H$ .

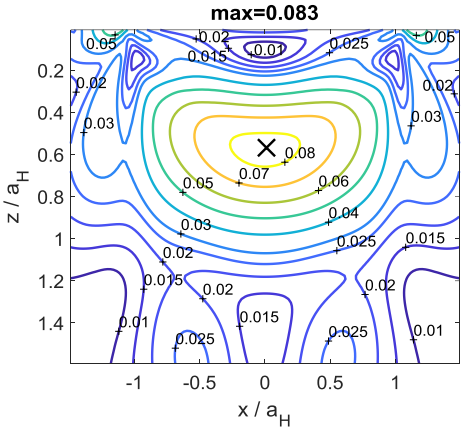


Fig. 3. Iso-contours of dimensionless equivalent von Mises stress due to plastic strains, $\sigma_{VM}^{r} / p_H$ .

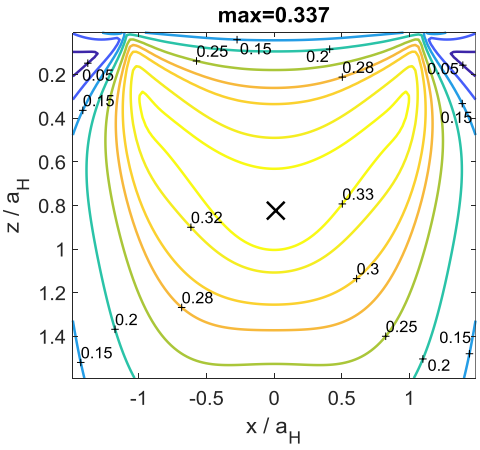


Fig. 4. Iso-contours of dimensionless total equivalent von Mises stress $\sigma_{VM} / p_H$ .

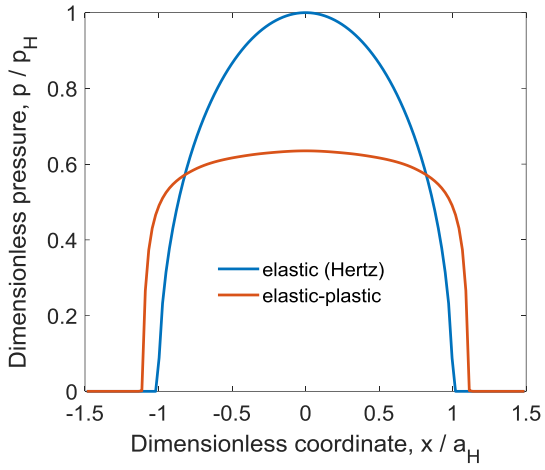


Fig. 5. The pressure profiles.

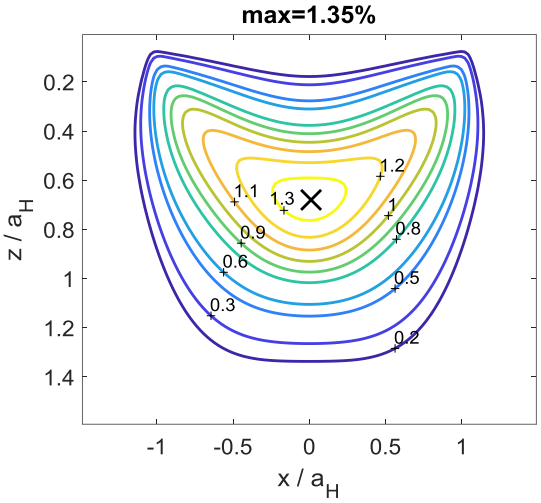


Fig. 6. Iso-contours of the plastic strain $e^{p}$ , [%].

## 7. CONCLUSIONS

An algorithm for the simulation of the elastic-plastic contact problem with power law isotropic hardening is assembled in this paper, with the Betti's reciprocal theorem as theoretical foundation for the application of superposition to plasticity. The contact pressure and the region with plastic strains are derived iteratively by trial-and-error, whereas the loading history is replicated by incremental load application, resulting in three nested loops. State-of-the-art numerical techniques based on the fast Fourier transform are implemented for the acceleration of convolutions computations.

The frictionless contact between a rigid spherical indenter and an elastic-plastic half-space is simulated. The numerical predictions suggest that:

1.The heart-shaped region with plastic strain is initiated in depth, and grows towards the half-space boundary. The maximum plastic strain is reached on the normal axis of the contact, at a certain depth, in the point of initial plastic yield. With further load increase, plastic strains are expected to reach the surface, thus

marking the transition to the perfectly (fully) plastic stage.

2.The residual stresses are one order of magnitude smaller than the ones induced by the contact pressure. However, their contribution results in an attenuation of the stresses due to the contact pressure. This results from comparison of shapes and levels of the stress iso-contours in figures 2 and 4. It can be concluded that some residual stress components have opposite signs to those of the pressure stresses. Thus, the residual stresses prevent further plastic flow.

3.All stress fields have maximum intensities on the central axis of the contact. In case of residual stresses, local maxima occur at the contact boundary, near the free surface.

4.The contact pressure is flattened compared with the purely elastic Hertzian framework, and the elastic-plastic contact radius is increased. The levelling of pressure can be attributed to: (1) the contribution of residual displacements, which acts to increase the contact conformity, and (2) the hardening of the elastic-plastic material.

Giving the modular structure of the computer program, the contact analyses can be extended to more complex scenarios, including friction and kinematic hardening.

## 8. REFERENCES


1. Jacq C., Nelias D., Lormand G., Girodin D., (2002), *Development of a Three-Dimensional Semi-Analytical Elastic-Plastic Contact Code*, ASME J. Tribol., 124, 653–667.
2. Brebbia L. C., (1980), *The Boundary Element Method for Engineers* (London: Pentech Press).
3. Mayeur C., (1995), *Modelisation du contact rugueux elastoplastique* (PhD Thesis, INSA Lyon, France).
4. Wang F., Keer L. M., (2005), *Numerical Simulation for Three Dimensional Elastic-Plastic Contact With Hardening Behavior*, ASME J. Tribol., 127, 494–502.
5. Boucly V., Nélias D., Liu S., Wang Q. J., Keer L. M., (2005). *Contact Analyses for Bodies With Frictional Heating and Plastic Behavior*, ASME J. Tribol., 127, 355 – 364.
6. Liu S., Wang Q., (2005), *Elastic Fields due to Eigenstrains in a Half-Space*, ASME J. Appl. Mech., 72, 871–878.
7. Boucly V., Nélias D., Green I. (2007), *Modeling of the Rolling and Sliding Contact Between Two Asperities*, ASME J. Tribol., 129, 235 - 245
8. Nélias D., Boucly V., Brunet M., (2006), *Elastic-Plastic Contact Between Rough Surfaces: Proposal for a Wear or Running-in Model*, ASME J. Tribol., 128, 236 - 244.
9. Nélias D, Antaluca E, Boucly V, Crețu S (2007), *A Three-Dimensional Semianalytical Model for Elastic-Plastic Sliding Contacts*, ASME J. Tribol., 129, 761 – 771.
10. Nélias D., Antaluca E., Boucly V., (2007), *Rolling of an Elastic Ellipsoid Upon an Elastic-Plastic Flat*, ASME J. Tribol., 129, 791 - 800.
11. Chen W. W., Liu S., Wang Q. J., (2008), *Fast Fourier Transform Based Numerical Methods for Elasto-Plastic Contacts of Nominally Flat Surfaces*, ASME J. Tribol., 75, 011022.
12. Chen W. W., Wang Q. J., (2008), *Thermomechanical Analysis of Elastoplastic Bodies in a Sliding Spherical Contact and the Effects of Sliding Speed*, Heat Partition, and Thermal Softening, ASME J. Tribol., 130, 041402.
13. Chen W. W., Wang Q. J., Wang F., Keer L. M., Cao J., (2008), *Three-Dimensional Repeated Elasto-Plastic Point Contacts, Rolling, and Sliding*, ASME J. Tribol., 75, 021021.
14. Chen W. W., Zhou K., Keer L. M., Wang Q. J., (2010), *Modeling elasto-plastic indentation on layered materials using the equivalent inclusion method*, Int J. Solids Struct., 47(20), 2841-2854
15. Chaise T., Nélias D., (2011), *Contact Pressure and Residual Strain in 3D Elasto-Plastic Rolling Contact for a Circular or Elliptical Point Contact*, ASME J. Tribol., 133, 041402.
16. Wang Z., Jin X., Liu S., Keer L. M., Cao J., Wang, Q., (2013), *A new fast method for solving contact plasticity and its application in analyzing elasto-plastic partial slip*, Mechanics of Materials, 60, 18-35.
17. Johnson K. L., (1996)., C*ontact Mechanics* (Cambridge: University Press).
18. Polonsky I. A., Keer L. M., (1999), *A New Numerical Method for Solving Rough Contact Problems Based on the Multi-Level Multi-Summation and Conjugate Gradient Technique*, Wear, 231, 206–219.
*19.* Liu S. B., Wang Q., Liu G., (2000), *A Versatile Method of Discrete Convolution and FFT (DC-FFT) for Contact Analyses, Wear, 243(1–2), 101–110.*
20. Liu S., Wang Q., (2001), *Studying Contact Stress Fields Caused by Surface Tractions With a Discrete Convolution and Fast Fourier Transform Algorithm*, ASME J. Tribol., 124, 36-45.
21. Spinu S., (2013), *A refined numerical solution to the inclusion problem*, Mechanika, 19(3), 252-259.


Received: May 8, 2022 / Accepted: December 15, 2022 / Paper available online: December 20, 2022 